Eur. Phys. J. B **56**, 291–295 (2007)
DOI: 10.1140/epjb/e2007-00138-y

THE EUROPEAN PHYSICAL JOURNAL B

Statistical analysis of shear cracks on rock surfaces

J.A. Åström[a]

CSC - IT-center for science, P.O. Box 405, 02101 Esbo, Finland

Received 23 November 2006 / Received in final form 22 March 2007
Published online 16 May 2007 –

Abstract. A set of 3873 cracks on exposed granite rock surfaces are analyzed in order to investigate possible fracture mechanisms. The fracture patterns are compared with the Mohr-Coulomb and the Roscoe fracture models, which can be combined into a single fracture scheme. A third model for comparison is based on interacting 'penny-shaped' micro cracks introduced by Healy et al. [Nature **439**, 64 (2006)]. The former models predict a bimodal fracture angle distribution, with two narrow peaks separated by $60^\circ - 90^\circ$ symmetrically on both sides of the direction of the largest principal stress, while the latter predicts a single broader peak in the same direction with standard deviation in the range $15^\circ - 20^\circ$. The crack length distributions seem consistent with numerical simulation, whereas the fracture patterns are Euclidean rather than fractal. The statistical analyses indicate that none of the models fully describe the fracture patterns. It seems that natural shear fractures easily become a complex combination of different fracture mechanisms.

PACS. 62.20.Mk Fatigue, brittleness, fracture, and cracks – 61.43.-j Disordered solids

1 Introduction

Crack patterns formed during fracture of brittle material are highly complex structures. There are several reasons for this complexity. Brittle material fracture through cracks which appear at locations where the stress exceeds the local fracture threshold [2]. Once cracks have been formed an enhanced stress concentration form at crack tips making the cracks unstable. According to the Griffith criterion for crack propagation, cracks longer than a critical length are unstable while shorter cracks remain stable for a given tensile stress [1]. Once cracks propagate they are prone to branching and splitting [3]. Furthermore, all brittle materials that appear in nature include some kind of flaws, impurities, grains or micro-cracks arranged in more or less random patterns. Such heterogeneities often act as origins of cracks and they may also alter crack propagation directions locally. Cracks also strongly affect the stress field over large areas which induce spatial correlations between cracks [4].

In spite of the complexity, there are some models, of shear fracture in particular, which rather well describe at least laboratory experiments [5]. Shear fracture patterns that appear in nature are much less controlled and thereby usually more difficult to understand. In this investigation a set of 3873 cracks on granite surfaces are used for testing three different shear fracture models (Mohr-Coulomb, Roscoe and Healy). It is demonstrated that none of the models are sufficient to explain the fracture patterns on their own, though the Roscoe model seems to best catch parts of the observed patterns. A linear combination of different fracture processes with different shear fracture mechanisms and boundary conditions would probably be sufficient to explain the observed patterns. The application of shear fracture for granite is particularly important because of its obvious connection to large-scale shear fracture in tectonic fault zones and the related earthquake hazard.

In very general terms, fractures can be divided into tensile and shear fracture. If the three eigenvalues of the stress tensor are denoted by σ_1, σ_2 and σ_3 the hydrostatic pressure (σ) on a body is $\sigma \equiv -(1/3)\sum_i \sigma_i$ (with $i = 1, 2, 3$). If σ is negative, i.e. 'negative pressure', then fracture will be tensile with crack surfaces being torn apart by the body tension. With a positive pressure it is usually very difficult to fracture a body unless it contains voids or pores to some extent. In the case of compression it is not the pressure but the deviatoric or shear stress ($\sigma_i - \sigma_j$, $i \neq j$) that is responsible for fracture. Assuming that $|\sigma_1| < |\sigma_2| < |\sigma_3|$, shear fracture will most likely first appear along a plane parallel to the eigenvector of σ_2. In this case, fracture means that the body parts will slide on each other along such a plane. Any plane parallel to σ_2 will experience a compressive normal force N and a tangential shear force S. At the initial stage of fracture a crack line must be formed and this demands that the cohesive forces k of the material must be overcome to form a crack. Once a crack is formed, slippage between the planes will occur if $S > \eta N$, where η is the friction coefficient of the material (i.e. the 'effective' friction coefficient, which may vary

[a] e-mail: astrom@csc.fi

depending on the fracture geometry). Shear fracture will thus occur along a plane for which $S > k + \eta N$. The shear and normal stresses on a plane oriented at an angle θ_{m-c} to σ_3 are given by

$$S = \cos(\theta_{m-c}) \sin(\theta_{m-c})(\sigma_3 - \sigma_1) \quad (1)$$

$$N = \cos^2(\theta_{m-c})\sigma_3 + \sin^2(\theta_{m-c})\sigma_1. \quad (2)$$

Maximizing $S - \eta N$ with respect to θ_{m-c} gives that shear fracture will appear along a plane oriented at an angle $\theta_{m-c} = (\pi/2 - \text{atan}(\eta))/2$ to the direction σ_3. η is typically in the range 0.5–0.7 for various kinds of rocks, which gives $\theta_{m-c} \approx 30°$. This is the result of the Mohr-Coulomb shear fracture model.

The fracture model of Roscoe [6] differs slightly from the Mohr-Coulomb model. In the Roscoe model the shear fracture angle is $\theta_r = (\pi/2 - \psi)/2$, where ψ is the angle of dilation, which is determined *not* by the normal and tangential forces on a plane *before* fracture as in the Mohr-Coulomb model, but by the incremental plastic strains at the failure point (σ_i^p). ψ is given by

$$\sin(\psi) = -\frac{d\sigma_1^p + d\sigma_3^p}{|d\sigma_1^p - d\sigma_3^p|}. \quad (3)$$

The interpretation of ψ is that for $\psi = 0$ the material preserves volume during plastic strain, while it expands to some extent for $\psi > 0$. The extension of the material takes place due to opening of cracks and sliding along rough crack surfaces. This is why the angle is called the dilation angle. It is usually rather small (0°–10°).

Shear fracture of rock changes with temperature and pressure. At low temperatures and pressures the material is quite brittle while at high temperatures and pressures it become more ductile. Such changes will alter both θ_{m-c} and θ_r, but the Mohr-Coulomb and Roscoe fracture models are still applicable. It should also be noticed that the Mohr-Coulomb and Roscoe fracture models do not exclude each other. The material yield may be determined by the Mohr-Coulomb fracture criterion, while the plastic strain may be governed by the Roscoe model.

For a positive σ, homogeneous compact material is fractured only through shear fracture as described above. This changes if the material is not compact but contains small micro-cracks or voids. This is rather well demonstrated by a stress field around a 2D circular hole under compression which may be solved for. In cylindrical coordinates the components $(\sigma_{rr}, \sigma_{\phi\phi}, \sigma_{r\phi})$ become [7]

$$\sigma_{rr} = \frac{\sigma_{inf}}{2}\left(1 - \frac{a^2}{r^2}\right) + \frac{\sigma_{inf}}{2}\left(1 - \frac{4a^2}{r^2} + \frac{3a^4}{r^4}\right)\cos(2\phi) \quad (4)$$

$$\sigma_{\phi\phi} = \frac{\sigma_{inf}}{2}\left(1 + \frac{a^2}{r^2}\right) - \frac{\sigma_{inf}}{2}\left(1 + \frac{3a^4}{r^4}\right)\cos(2\phi) \quad (5)$$

$$\sigma_{r\phi} = -\frac{\sigma_{inf}}{2}\left(1 + \frac{2a^2}{r^2} - \frac{3a^4}{r^4}\right)\sin(2\phi), \quad (6)$$

where a is the radius of the hole and σ_{inf} is the stress in the radial direction at $\phi = 0$ far from the hole. For a compressive stress ($\sigma_3 < \sigma_1 < 0$), it can be extracted from equation (5) that tension easily becomes positive within an interval symmetrically around the direction of σ_3 in the direction of σ_1 (e.g. by choosing σ_3 as the direction $\phi = 0$ and σ_1 as the direction $\phi = -\pi/2$ and adding the two stress components equation (5) for the two orthogonal directions). This means that in a compressive stress situation tensile fracture is possible near voids or micro cracks. This changes the fracture behavior quite radically. In particular it means that fracture planes are likely to appear parallel to the maximum principle stress direction and within an interval symmetrically located around this direction. This is in sharp contrast to the Mohr-Coulomb or Roscoe fracture, where the fracture planes only appear at the angles $\pm\theta_{m-c}$ or $\pm\theta_r$ from the same direction (or maybe at an angle that is somewhere between θ_{m-c} and θ_r [8]).

The interval in which the stress is tensile depends on the shape of the crack. Probably, the best estimate of the interval width for typical micro-crack is that of Healy et al. [9] using the solution of Eshelby [10] for "penny-shaped" cracks. This model gives that the penny-shaped cracks interact to strengthen the tensile stress within ±26° from each other. The Healy model thus predicts a set of cracks with orientation distributions within an interval of 52°.

It is not only the orientation angle of the cracks in a fracture pattern that is a useful measurable quantity. Also the length of the individual cracks can be estimated. This quantity cannot be completely unambiguously determined because in principle, it is impossible to determine where a new crack begins, where another one stops or if it is a single crack that turns abruptly.

In a numerical model based on the Mohr-Coulomb and Roscoe model fracture, Poliakov and Herrmann [11] determined the fractal dimension (box counting algorithm) and the length distribution of a shear crack pattern. In this model, the strength of the material (i.e. the yield point) is determined by the Mohr-Coulomb model while the plastic strain is determined by the Roscoe's model through the dilation angle ψ. As could be expected, the orientation angle of the shear fracture was found within the interval $[\theta_{m-c}, \theta_r]$. The crack length distribution was found to be a power-law with the exponent 2.1 ± 0.1, and the geometrical fractal dimension of the cracks to be 1.7 ± 0.1.

In order to test the results of the models above, a set of four crack patterns were analyzed. The fracture patterns contained a total of 3873 detected crack lines, ranging in size from a few tens of centimeters to over ten meters. Also the dip angles of the fracture planes were extracted. Since the angles for a clear majority were quite close $\pi/2$, we could use the 2D patterns to estimate the angles between the crack planes. The cracks were measured by on-site field measurements on four exposed granite surfaces of approximately 30 m × 30 m a few kilometers apart from each other near the Äspö Hard Rock Laboratory in Oskarshamn [13–15]. The crack patterns are displayed in Figure 1. The cracks are divided into connected discrete line segments with a resolution of about 10 cm. The

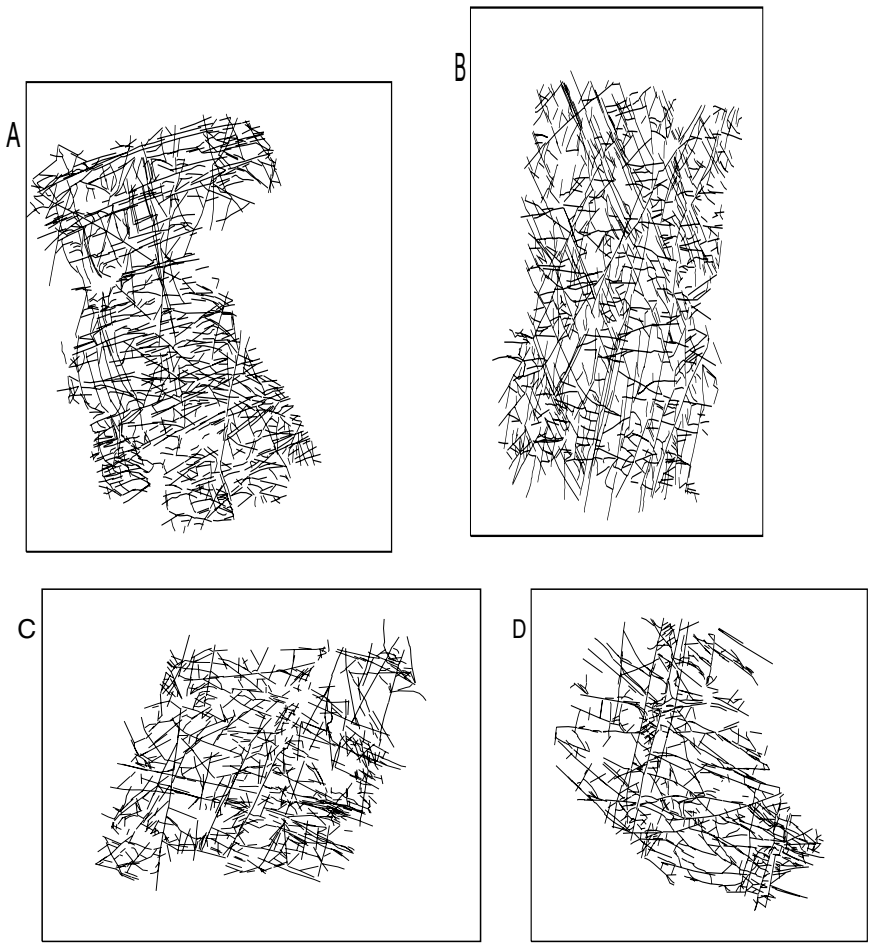

Fig. 1. Four crack patterns on exposed granite rock surfaces from the east coast of Sweden near the Äspö Hard Rock Laboratory in Oskarshamn. The approximate dimensions of the crack patterns are 30 m × 30 m. Cracks down to a few tens of centimeters are recorded. The longest cracks are over 10 m.

cracks are fairly straight and the orientation angles are thus well defined. At intersections a crack typically terminates or continues in approximately the same direction on the other side, which means that cracks can easily be distinguished.

The crack angle distributions of the crack patterns are displayed in Figure 2. This figure shows the total crack length within small angle intervals of the cracks in Figure 1. I.e. for each crack an orientation angle is defined as the orientation angle of the line between the end points of the crack, and the sum of the lengths of the cracks with orientation between θ and $\theta + \delta\theta$ is plotted in Figure 2 as a function of θ.

From Figure 2 it is quite clear that some distinct peaks in the crack orientation angles can be identified. Gaussian distribution functions are fitted to these peaks and the fits are displayed with broken lines in Figure 2. The angles of the maxima and the standard deviations of the peaks are listed in Table 1. The two last columns of this table show the minimum angle between the peak maxima, and the estimated direction of the largest principal stress, where applicable.

Fitting a Gaussian distribution does not give an exact determination of the interval of the orientation angles. If there is a 'noise level' in the data, the width of the Gaussian at this level may function as the interval width. Then roughly, the Healy interval of maximum $\pm 26°$ corresponds to a standard deviation of about 15°–20°. This means that three peaks (in B, C and D) are broad enough to be possible Healy fractures, while six peaks are too narrow. The crack patterns A, C and D all contain only two peaks and minimum angles which fit well the Roscoe angle ($2\theta_r \in [80°, 90°]$) for A and C and perhaps also for D (D also fits the Arthur angle $(\theta_{m-c} + \theta_r)/2$ [8]).

This means that A can be interpreted as a pure Roscoe model fracture. C can also be identified as a Roscoe fracture but with one peak broad enough to be a Healy fracture. D is possibly also a Mohr-Coulomb/Roscoe fracture but has one peak broad enough to be a Healy fracture. B is the most complicated case with two high peaks and possibly one low peak between them. The low peak is broad enough to be a Healy fracture, but the other two are too narrow. The angle between the two narrow peaks is only 41°, which is quite small even to be a Mohr-Coulomb model angle.

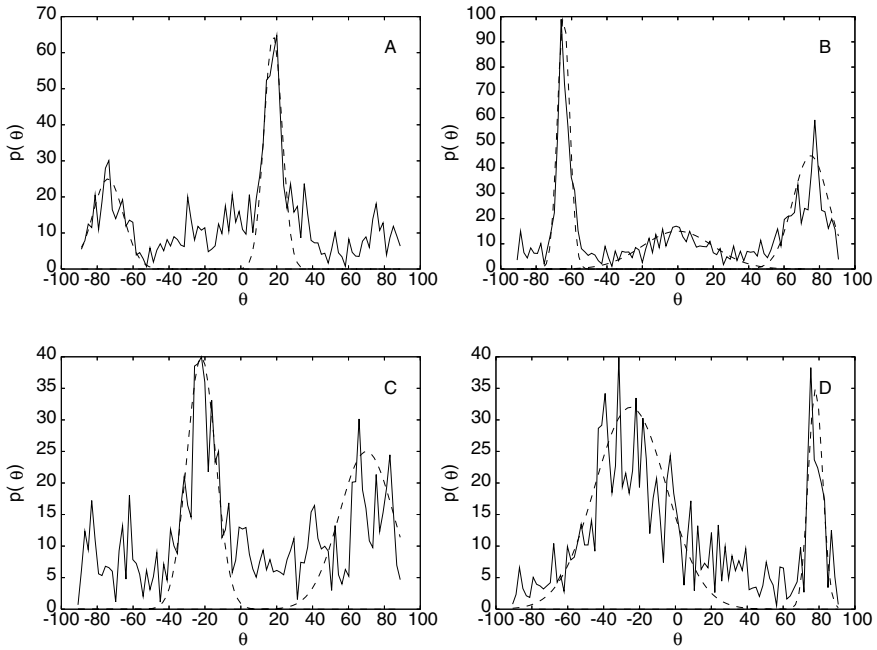

Fig. 2. (A–D) The orientation angle distribution (total length of cracks with average orientation between θ and $\theta + \delta\theta$) for the fracture patterns in Figure 1. $\theta = 0$ corresponds to a horizontal crack in Figure 1.

Table 1. Location (in degrees) of the orientation distribution maxima (Max) displayed in Figure 2 (A, B, C and D, respectively), and the standard deviation (std) of the fitted Gaussian distributions. The two last columns give the minimum angle between the peaks, and the estimated direction of the largest principal stress for A, C, D, for which it is possible to be extracted.

Fig.	Max, std	Max, std	Max, std	Min ang	σ_3
A	18, 5	–74, 8.5	–	88	62
B	75, 10	0, 20	–64, 3.5	75, 64, 41	–
C	70, 15	–22, 8	–	88	–66
D	–25, 20	78, 4	–	77	–63.5

The length distribution of the cracks in Figure 1 are compared with the Mohr-Coulomb/Roscoe model results of reference [11] in Figure 3. The line is the power-law $n(l) \propto l^{-2.1}$. The results are consistent but the length scale range of the measured fracture lines is too small to prove scale invariance. The power exponent being close to 2 is interesting because this value gives a constant area density of cracks at any length scale (i.e. the average number of cracks of length between l and $l + \delta l$ in an area of size l^2 is independent of l). In this respect the crack patterns are self-similar. It seems, however, that the power-law $n(l) \propto l^{-2.1}$ cannot be extended to large scale fracture zones (10^2–10^5 m), but instead, fitting a power-law to the entire length range gives $n(l) \propto l^{-3}$ [15].

Finally, the dimension of the crack patterns are determined using the box-counting algorithm. In contrast to reference [11] no fractality is detected. The number of boxes containing a crack line scales as $1/l_b^2$ for large boxes and for small boxes as $1/l_b$, where l_b is the side length of the boxes. This means that on large scales the fracture patterns have a dimension similar to their Euclidean dimension ($D = 2$), while the ($D = 1$) structure of the crack line becomes visible on small scales. In a log-log plot (Fig. 4) no power-law regime can be detected in the cross-over between these two limits. It is possible that such a regime could be detected if smaller cracks were included in the crack patterns, but the data available at the moment does not indicate any fractality in the crack patterns.

The cross-over point between $D = 2$ and $D = 1$ occurs at about $1/l_b \approx 50$, which corresponds to a crack length of about half a meter. This defines the typical separation distance between cracks and thus also the coarseness of the crack network [12].

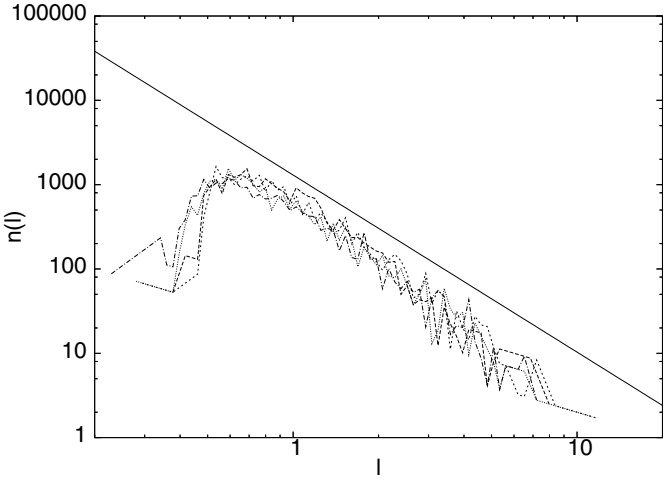

Fig. 3. The length distribution of crack lines for the four fracture patterns in Figure 1. The straight line is the result of reference [11] $n(l) \propto l^{-2.1}$.

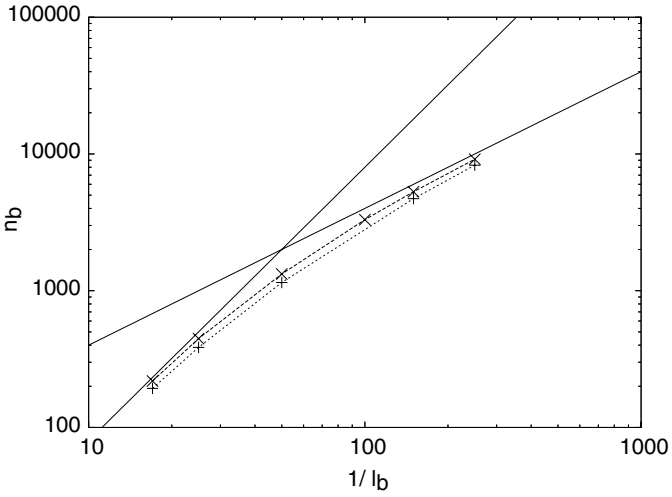

Fig. 4. The number of boxes n_b containing a crack line as function of $1/l_b$, where l_b is the side length of the boxes covering the crack pattern. The steeper straight line slope is $n_b \propto 1/l_b^2$ and the moderate slope is $n_b \propto 1/l_b$.

An interesting observation is that the orientation angle distribution maxima does not coincide for the four sets of cracks even though they are located within a few kilometers from each other. C and D seem to have the same orientation, but A and B differ from these two and from each other. A plausible explanation is that both C and D are located east of a large shear zone (called the Äspö shear zone), while A and B are located west of this zone. This would indicate that at least some of the crack patterns have been formed after the shear zone. The formation of a shear zone effectively releases shear stress [16,17] and therefore, one would expect that the principal stress directions in its vicinity after its formation are along the shear zone and perpendicular to it. Right before the formation of the zone (that is, on a geological time scale) one would, conversely, expect that shear stress across the zone is at its maximum. The orientation of the Äspö shear zone is roughly 60° near the crack pattern locations. The expected principal stress directions, after the shear zone formation, would then be roughly 60° and –30°. The former angle coincides with A if it is a Mohr-Coulomb/Roscoe fracture. The orientation maxima for C and D does not seem to be related to the shear zone direction.

Based on the orientation angle analysis summarized in Table 1 it is impossible to make a clear distinction of the dominating shear fracture mechanism responsible for the crack patterns in Figure 1. The results of the statistical analysis presented here are perhaps a little in favor of the Roscoe model fracture. The general conclusion must, however, be that none of the Mohr-Coulomb, Roscoe or Healy model is sufficient to fully explain the crack patterns in Figure 1 on their own. It is likely that the crack patterns are results of a non-trivial combination of several involved mechanisms. In particular, it seems possible that a Mohr-Coulomb/Roscoe fracture mechanism has dominated in general, but that interacting micro-cracks have caused quite a lot of fluctuations in the crack plane directions, thus explaining the relative broad peaks in the orientation angle distributions. It also seems likely that the approximately 10^9 years old granite has undergone several chronologically separate fractures under different loading conditions forming the patterns detected today [14]. This may, at least in part, explain why no fractality is detected.

Introducing a fracture model with N different and separate fracture processes that leads to a fracture pattern that is a linear combination of the crack pattern of the different models and with different weights and loading conditions would certainly be sufficient to reproduce the observed crack orientation distributions. As already mentioned above: A can be interpreted as a pure Roscoe model fracture, B as a combination of Healy and Mohr-Coulomb fractures, and both C and D as a Mohr-Coulomb/Roscoe fracture with one Healy fracture orientation angle maxima coinciding with one of the M-C/R peaks. This level of detailed interpretation of the fracture patterns are, however, not much more than speculations of the origin of very complex patterns.

References

1. A.A. Griffith, Phil. Trans. R. Soc. A **221**, 163 (1921)
2. *Statistical models for the fracture of disordered media*, edited by H. Herrmann, S. Roux (North-Holland, Amsterdam, 1990)
3. J. Fineberg, M. Marder, Phys. Rep., 313 (1999)
4. J.A. Åström, Advances in Physics **55**, 247 (2006)
5. J.M. Ramsey, F.M. Chester, Nature **428**, 63 (2004)
6. K. Roscoe, Geotechnique **20**, 170 (1970)
7. G. Kirsch, Zeitschrift der Vereines Deutscher Ingenieure **42**, 797 (1898)
8. J. Arthur, T. Dunstan, Q. Al-Ani, A. Assadi, Geotechnique **27**, 53 (1977)
9. D. Healy, R.R. Jones, R.E. Holdsworth, Nature **439**, 64 (2006)
10. J.D. Eshelby, Proc. R. Soc. Lond. A **241**, 376 (1957); J.D. Eshelby, Proc. R. Soc. Lond. A **252**, 561 (1959)
11. A.N.B. Poliakov, H.J. Herrmann, Geophys. Res. Lett. **21**, 2143 (1994)
12. D.L. Turcotte, *Fractals and chaos in geology and geophysics* (Cambridge Univ. Press, 1997)
13. The fracture patterns have been extracted by SKB ltd. which is the Swedish company responsible for nuclear waste management. Information on SKB and the Äspö Hard Rock Laboratory can be found under `http://www.skb.se`
14. J. Hermanson, O. Forssberg, A. Fox, P. La Pointe, SKB-report: SKB R-05-45 (available at `http://www.skb.se`) Statistical model of fractures and deformation zones. Preliminary site description, Laxemar subarea, version 1.2 (2005)
15. C. Darcel, P. Davy, O. Bour, J.-R. De Dreuzy, SKB-report: SKB R-04-76 (available at `http://www.skb.se`) Alternative DFN model based on initial site investigations at Simpevarp (2004)
16. M.J. Zoback, V. Zoback, J. Mount, J. Eaton, J. Healy, Science **238**, 1105 (1987)
17. J.A. Åström, H.J. Herrmann, J. Timonen, Eur. Phys. J. E **4**, 273 (2001)